Effect of radiation pressure on the Hill's curves for two binary systems in ERTBP

A. Chakraborty[1], A. Narayan[2]
[1] Department of Mathematics, Bhilai Institute of Technology, Durg, C. G., India, 491001
aninditachakraborty@bitdurg.ac.in
[2] Department of Mathematics, Darbhanga College of Engineering Department of Science and Technology Goverment of Bihar
ashutoshmaths.narayan@gmail.com
(Submitted on 6.01.2024; Accepted on 17.04. 2024)

Abstract. In this paper we have undertaken the study of systems with two radiating primaries in the framework of an elliptic restricted three-body problem, where the orbits of the two massive bodies about each other are assumed to be elliptic and the mass of the third body is negligible. We have made a comparative study of analytical and numerical results for the position of equilibrium points in the case of two binary systems, *Eta Cassiopeiae* and *Gliese* 65. We have further studied the Hill's curves and observed the pulsation of the curves with the true anomaly and change in size of the forbidden regions (the size of the interior forbidden region decreases but the region enclosed by the larger boundary enclosing all primaries and equilibrium points increases in size) of motion with change in radiation pressure of the two primaries. We did a study of Basin of Attraction for the planar equilibrium points and found that the size of basins changes (decreases for L_2-L_5 and increases for L_1) with the value of radiation pressure q_1 of the first primary, whereas the symmetry of the basin of attraction of L_1 was observed to be distorted with decrease in radiation pressure q_2 of the second primary.
Key words: Restricted Three-body Problem, Fractal basin of attraction, Hill's curve, Binary systems

Introduction

Stellar dynamical problems examine how radiating bodies affect particles of infinitesimal mass. It was found that the most dominant force affecting the dynamics of an infinitesimal mass is the force of radiation pressure and not the gravitational force. When the third infinitesimal mass in a system with radiating primaries has substantial sailing capacity (for example, cosmic dust, stellar wind etc), then the classical planar circular restricted three-body problem (CRTBP) cannot be used to study the dynamics of such systems. Thus it was proposed to modify the classical RTBP by superposing a radiative repulsion field with the gravitational field of the luminous primaries. The study of the effect of radiation pressure when one or both the primaries of the system are radiating sources in Circular Restricted Three-Body Problem(CRTBP) was first undertaken by Radzievskii [1950, 1953] and is known as photogravitational RTBP.

Schuerman [1980] studied the inclusion of the radiation force in the restricted three-body problem by observing the effect of the major radial components of the pressure force. For this model he considered the case of a β-particle in the vicinity of two luminous massive bodies. He showed that the position of L_4 and L_5 equilibrium points may be anywhere within the union of two circles which are centered on the radiating primaries and the circles have equal radii which is equivalent to the separation of the two primaries.

In the previous century, several authors have studied the various aspects of the photogravitational restricted three-body problem. Some of the contributions are Kunitsyn and Perezhogin [1978], Bhatnagar and Chawla [1979],

Kunitsyn and Tureshbaev [1985] etc. One interesting sub-topic of the photogravitational restricted three-body problem, undertaken by several scientists in this century, is the computation of families of periodic orbits (Kalantonis et al. [2006], Kalantonis et al. [2008]). Alzahrani et al. [2017] have considered the infinitesimal mass to be moving in the gravitational field of an irregular asteroid and radiating primaries in photogravitational restricted three-body problem. They established the necessary and sufficient conditions for finding the three collinear points and proved the existence of these points and triangular equilibrium points. Singh and Haruna [2020] studied the position and stability of the triangular equilibrium points when both primaries are radiating and considered as heterogeneous spheroid with three layers of different densities. In their model, the effects of small perturbations in the Coriolis and centrifugal forces and potential from a belt (circumbinary disc) were also included. Numerical methods were employed to determine the positions and the linear stability of the coplanar equilibrium points. Alrebdi et al. [2022] also investigated the equilibrium dynamics of the restricted three-body problem with equally massed prolate radiating bodies using numerical methods. Their result established that both radiation pressure and prolate-ness are highly influential on the equilibria of the system.

Danby [1964] studied the Elliptic Restricted Three-Body Problem (ERTBP) and used numerical integration to determine the linear stability of the elliptic Lagrange orbits. Selaru and Cucu-Dumitrescu [1995] investigated the asymptotic disturbance approximations in the planar, elliptic restricted problem of three bodies in the neighborhood of a Lagrangian equilateral position for motions of an infinitesimal point mass with small amplitudes. The study of Photo-gravitational Elliptical Restricted Three-Body Problem was undertaken by Ammar [2008]. He proved that the radiation pressure slightly reduces the effective mass of the Sun and changes the location of the Lagrangian points. Kumar and Ishwar [2011] studied the photogravitational ERTBP and derived the location of the collinear libration points analytically. Further, Aliroma et al. [2019] proved that the size of the stability region depends on the eccentricity of the orbits in addition to other perturbations like radiation pressure.

In some recent studies, we observed the study of photogravitational ERTBP with reference to binary systems. Narayan and Singh [2014, 2014a] studied the ERTBP where both primaries are luminous to find the position and stability of the equilibrium points. Narayan and Singh [2014b] also studied the resonance stability of these points. The work done by Singh and Isah [2021] analyzed the effects of radiation pressure and triaxiality of the two radiating primaries on the location of equilibrium points, where the primaries are assumed to be surrounded by a circum-binary belt in the framework of elliptic restricted three-body problems. They concluded that stability of the orbit of the third body in the neighborhood of collinear libration points was affected by triaxiality, radiation and the gravitational potential of the belt.

In this paper we have extended the works Narayan and Singh [2014] and Narayan and Singh [2014b]. First, we compared the analytically obtained values of the position of equilibrium points, as given in these papers, with numerical results using graphical representation. We then studied Hill's region on the ecliptic plane. Finally, we made a study of the Fractal basin of attraction for planar equilibrium points, comparing the effect of the radiation pressure on the basin.

We did the study mainly by theoretically applying the results obtained for two binary star systems. The first binary system we studied is the Eta Cassiopeiae (ηCas) in the northern constellation of Cassiopeia. Eta Cassiopeiae's two components, i.e. $\eta Cas\ A$(Achird) and $\eta Cas\ B$ are orbiting around each other over a period of 480 years in highly eccentric orbits and are separated from each other by an average distance of 72 AU (Strand [1969]). The second binary system is Gliese 65 (or Luyten 726-8), which is one of the Earth's nearest neighbours. The two components of the system, Gliese $65A$ (BL Ceti) and Gliese $65B$ (UV Ceti), orbit one another every 26.5 years in highly eccentric orbits. The distance between the two stars varies from 2.1 to 8.8 astronomical units (Luyten [1949]).

1 Equation of motion

The model proposed in this study comprises of two radiating primaries located on the rotating-pulsating $\bar{x}-axis$ at the points $S_1(\bar{x}_1, \bar{y}_1, \bar{z}_1)$ and $S_2(\bar{x}_2, \bar{y}_2, \bar{z}_2)$, and revolving around their common center of mass in elliptic orbits with variable angular velocity $\underline{\dot{f}} = (0, 0, \dot{f})$, with respect to the inertial frame XYZ. The model studies the motion of the infinitesimal mass P in the proximity of the two primaries as shown in Figure 1.

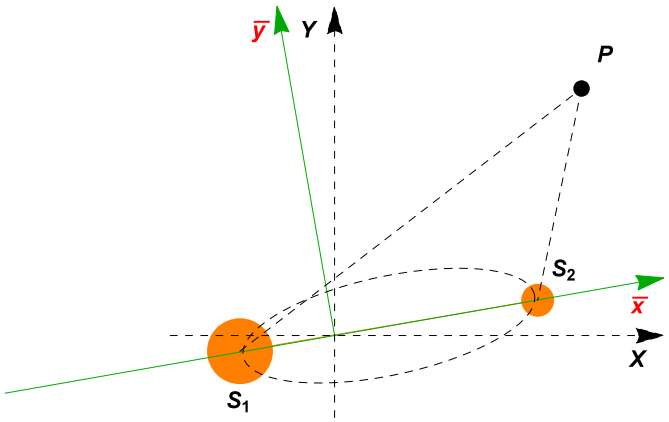

Fig. 1. The model for Elliptic Restricted Three Body Problem

The coordinate system used to frame the equations is the pulsating, rotating barycentric system $\bar{x}\bar{y}\bar{z}$. The $\bar{z}$-axis is assumed to be parallel to the $Z-$axis of the inertial reference frame.

To begin with, we write the equation of motion of the infinitesimal mass in the inertial reference frame:

$$\begin{aligned}
\frac{d^2X}{dt^2} &= -G\left[\frac{m_1(X-X_1)q_1}{R_1^3} + \frac{m_2(X-X_2)q_2}{R_2^3}\right];\\
\frac{d^2Y}{dt^2} &= -G\left[\frac{m_1(Y-Y_1)q_1}{R_1^3} + \frac{m_2(Y-Y_2)q_2}{R_2^3}\right];\\
\frac{d^2Z}{dt^2} &= -G\left[\frac{m_1(Z-Z_1)q_1}{R_1^3} + \frac{m_2(Z-Z_2)q_2}{R_2^3}\right].
\end{aligned} \tag{1}$$

Here, $R_i = \sqrt{(X-X_i)^2 + (Y-Y_i)^2 + (Z-Z_i)^2},\ i = 1, 2$ is the distance of the infinitesimal mass from the primaries, respectively, in this frame, and $q_i = 1 - \beta_i$ is the radiation pressure exerted by the stars. The dimensionless quantities β_1 and β_2 specify the effect of radiation pressure. It is defined as

$$\beta_i = \frac{3L_{*i}\bar{Q}'_{pr_i}}{16G\pi c m_i R_d \rho},\ \text{where } i = 1, 2. \tag{2}$$

Here, ρ is the density and R_d is the radius of the infinitesimal dust particle. m_i is the mass, L_{*i} is the stellar luminosity and $\bar{Q}'_{pr_i}$ is the dimensionless efficiency factor for the radiation pressure, averaged over the stellar spectrum. G is the gravitational constant and c is the speed of light in vacuum.

The polar equation of elliptic orbits, considered in ERTBP (Ammar [2008]), takes the form

$$r = \frac{a(1-e^2)}{1 + e\cos f}, \tag{3}$$

where f is the true anomaly of the smaller primary S_2 and e is the eccentricity of the elliptical orbit of both primaries.

The next step was to transform to a rotating coordinate system $Oxyz$ using the transformation

$$\begin{aligned}
X &= x\cos f - y\sin f;\\
Y &= x\sin f + y\cos f;\\
Z &= z.
\end{aligned}$$

Thus we have

$$\begin{aligned}
\ddot{x} - 2\dot{y}\dot{f} - y\ddot{f} - x\dot{f}^2 &= -G\left[\frac{m_1(x-x_1)q_1}{r_1^3} + \frac{m_2(x-x_2)q_2}{r_2^3}\right];\\
\ddot{y} + 2\dot{x}\dot{f} + x\ddot{f} - y\dot{f}^2 &= -G\left[\frac{m_1(y-y_1)q_1}{r_1^3} + \frac{m_2(y-y_2)q_2}{r_2^3}\right]\\
\ddot{z} &= -G\left[\frac{m_1(z-z_1)q_1}{r_1^3} + \frac{m_2(z-z_2)q_2}{r_2^3}\right]
\end{aligned}$$

In order to maintain the primaries in fixed positions, we transform to Nechville's coordinate system using the transformation

$$x = r\bar{x}, y = r\bar{y},\ z = r\bar{z},\ r_1 = r\bar{r_1} \text{ and } r_2 = r\bar{r_2},$$

where, the unit of length is chosen as the instantaneous distance between the primaries, namely r defined by (3), the independent variable is chosen to be the true anomaly f of the Keplerian motion, described by the smaller primary. Also, following the usual practice, we choose a system of units as: the gravitational constant is unity and the sum of the masses of the primaries is unity, i.e $m_1 + m_2 = 1$. We define

$$\mu = \frac{m_2}{m_1 + m_2}, \quad 1 - \mu = \frac{m_1}{m_1 + m_2}; \quad 0 < \mu < \frac{1}{2}.$$

Accordingly, the separation between the primaries will be constant and equal to one. Then, the position of the two primaries is determined by the coordinates $(\bar{x}_1, \bar{y}_1, \bar{z}_1) = (\mu, 0, 0)$, $(\bar{x}_2, \bar{y}_2, \bar{z}_2) = (1 - \mu, 0, 0)$.

We take the true anomaly, f, as the new independent variable rather than the time t. Then, using the relation $df/dt = 1/r^2$, the equations of motion of the particle $p(\bar{x}, \bar{y}, \bar{z})$ in this pulsating system, are given in the form:

$$\begin{aligned}
\bar{x}'' - 2\bar{y}' &= \Omega_{\bar{x}} = \frac{1}{1 + e\cos f}\omega_{\bar{x}};\\
\bar{y}'' + 2\bar{x}' &= \Omega_{\bar{y}} = \frac{1}{1 + e\cos f}\omega_{\bar{y}};\\
\bar{z}'' + \bar{z} &= \Omega_{\bar{z}} = \frac{1}{1 + e\cos f}\omega_{\bar{z}};
\end{aligned} \tag{4}$$

where

$$\begin{aligned}
\omega &= \frac{1}{2}(\bar{x}^2 + \bar{y}^2 - \bar{z}^2 e\cos f) + \frac{q_1(1-\mu)}{\bar{r}_1} + \frac{q_2\mu}{\bar{r}_2};\\
q_i &= (1 - \beta_i), \quad i = 1, 2,\\
\bar{r}_1 &= \sqrt{(x+\mu)^2 + y^2 + z^2}, \quad \bar{r}_2 = \sqrt{(x+\mu-1)^2 + y^2 + z^2}.
\end{aligned} \tag{5}$$

The prime ($'$) denotes the differentiation with respect to the true anomaly f.

2 Planar Equilibrium points

The points on the plane of motion of the primaries, where velocity and acceleration of the infinitesimal mass is almost zero, are called the equilibrium points or Libration points, or Lagrangian points.
The planar equilibrium points for the problem were derived analytically (Narayan and Singh [2014, 2014a]) solving the system of equations:

$$\Omega_{\bar{x}} = 0, \quad \Omega_{\bar{y}} = 0$$

These equations are obtained because at the libration points the velocity and acceleration of the infinitesimal mass is assumed to be zero and for planar equilibrium points we also take $\bar{z} = 0$.

The first three points which lie on $x-$axis are known as collinear points. For the collinear equilibrium points we have $\bar{y} = 0$. Thus, we get the equation

$$\Omega_{\bar{x}} = \bar{x} - \left(\frac{q_1(1-\mu)(\bar{x}+\mu)}{|\bar{x}+\mu|^3} + \frac{q_2\mu(\bar{x}+\mu-1)}{|\bar{x}+\mu-1|^3} \right) = 0.$$

The solution of this quintic equation is obtained analytically by using series expansion as shown in detail by Narayan and Singh [2014a].

The two points $L_{4,5}$, which are positioned symmetrically above and below $x-$axis, are known as triangular equilibrium points and are obtained by solving the equations (Narayan and Singh [2014]):

$$\Omega_{\bar{x}} = \bar{x} - \left(\frac{q_1(1-\mu)(\bar{x}+\mu)}{\bar{r}_1^3} + \frac{q_2\mu(\bar{x}+\mu-1)}{\bar{r}_2^3} \right) = 0,$$
$$\Omega_{\bar{y}} = \bar{y} - \left(\frac{q_1(1-\mu)\bar{y}}{\bar{r}_1^3} + \frac{q_2\mu\bar{y}}{\bar{r}_2^3} \right) = 0.$$

The planar equilibrium points for the problem were derived analytically (Narayan and Singh [2014, 2014a]) solving the system of equations, as given below:

L_1 :

$\bar{x} = 1 - \mu - \rho_1, \ \bar{y} = 0$

where,

$$\rho_1 = \alpha_1 - \frac{1}{3}\left(\frac{1-2\beta_1/3}{1-4\beta_1/3}\right)\alpha_1^2 - \frac{1}{9}\left(\frac{1-8\beta_1/3+44\beta_1^2}{1-4\beta_1/3}\right)\alpha_1^3 + \cdots$$

$$\alpha_1 = \left(\frac{\mu(1-\beta_2)}{3(1-\mu)(1-4\beta_1/3)}\right)^{1/3}$$

L_2 :

$\bar{x} = 1 - \mu + \rho_2, \ \bar{y} = 0$

where,

$$\rho_2 = \alpha_2 + \frac{1}{3}\left(\frac{1+14\beta_1/3}{1+4\beta_1/3}\right)\alpha_2^2 - \frac{1}{9}\left(\frac{1-32\beta_1/3-28\beta_1^2}{1+4\beta_1/3}\right)\alpha_2^3 + \cdots$$

$$\alpha_2 = \left(\frac{\mu(1-\beta_2)}{3(1-\mu)(1+4\beta_1/3)}\right)^{1/3}$$

L_3 :

$$\bar{x} = -\mu - \rho_3,\ \bar{y} = 0$$

where,

$$\rho_3 = 1 - \frac{\beta_1}{3} - \frac{12}{7}\left(1 - \frac{5\beta_1}{3(7+\beta_2)}\right)\alpha_3 + \frac{12}{7}\left(1 - \frac{1054\beta_1}{144(7+\beta_2)}\right)\alpha_3^2 + \cdots$$

$$\alpha_3 = \frac{\mu}{(1-\mu)}$$

$L_4,\ L_5$:

$$\bar{x} = \frac{1}{2} - \mu + \frac{1}{2}\left((1-\beta_1)^{2/3} - (1-\beta_2)^{2/3}\right)$$

$$\bar{y} = \pm\sqrt{(1-\beta_1)^{2/3} - \frac{1}{4}\left((1-\beta_1)^{2/3} - (1-\beta_2)^{2/3}\right)^2}$$

Binary System	Mass of primary (m_i)	Eccentricity (e)	Distance between two the stars (a)	Mass ratio (μ)	Lumonisity
($\eta\ Cas$)	($\eta\ Cas\ a$) $= 0.972\ M_\odot$ ($\eta\ Cas\ b$) $= 0.57\ M_\odot$	0.497	71 AU	0.258126	($\eta\ Cas\ a$) $= 1.2321 L_\odot$ ($\eta\ Cas\ b$) $= 0.06 L_\odot$
Gliese 65	*Gliese* 65 A $= 0.1225\ M_\odot$ *Gliese* 65 B $= 0.1195\ M_\odot$	0.6185	8.8 AU	0.493802	*Gliese* 65A $= 0.00147 L_\odot$ *Gliese* 65B $= 0.00125 L_\odot$

Table 1. The data for ($\eta\ Cas$) system (Strand [1969]) and *Gliese* 65 system (Luyten [1949]).

To study the effect of the radiation pressure of the primaries on the position of the planar equilibrium points and to compare the position of the points as obtained analytically and numerically, we are applying the results of the analysis to two binary systems namely Eta Cassiopeia ($\eta\ Cas$) and Gliese 65. Table 1 lists the required parameters for the two binary systems. We have chosen these two systems as both of them have radiating primaries and are moving in highly eccentric orbits. However, the mass-ratio is very different in each case.

First, we tabulate the numerically obtained position of the equilibrium points for the two binary system in Table 2. From the values of the coordinates, both for triangular and collinear points, we note that the radiation pressure of both stars are effecting the position of the equilibrium points. However, the shift in the position is more prominent with decrease in radiation pressure of the first primary.

We have also compared the results obtained analytically by Narayan and Singh [2014, 2014a] with the numerical results for the two systems. Figures 2 and 3 show the change in the position of the equilibrium points for (η Cas) with change in value of q_2 and q_1, respectively. In these figures, the solid lines represent the position of the equilibrium points, obtained as a function of the mass ratio and the radiation pressure analytically.

The dotted curves show the shift in the equilibrium points as observed numerically, using Mathematica 10 software. Similarly, the Figures 4 and 5 are representations of equilibrium points for the $Gliese65$ system.

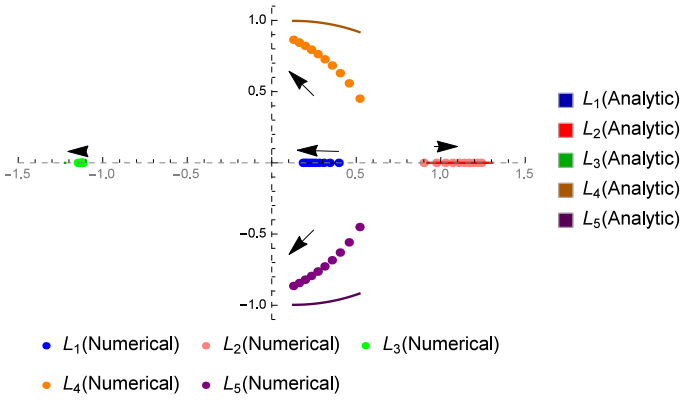

Fig. 2. The shift in the planar equilibrium points for (η Cas) system when q_2 is changed from 0.1 to 1 and $q_1 = 0.99$. The dots denote the points corresponding to the numerical calculation whereas the solid line shows the shift in position corresponding to analytically obtained expression.

Table 2 and Figures 2 to 5 clearly show that all the equilibrium points are dependent on the values of q_1 and q_2 for both binary star systems. However numerical calculations show that the effect of q_1 is least on L_2 and effect of q_2 is least on L_3. The arrow heads shown in the figures indicate the direction of shift with decrease in radiation pressure. We may also conclude that the triangular points are most prominently affected by radiation pressure in both cases. These results are in concurrence with the result obtained by Ammar [2008].

We note that the shift in position of the collinear point L_1, obtained as a function of q_2, is almost coincidental with the numerical results for both systems. But the analytic value of the collinear point L_2 and L_3 is an overestimation of the numerically obtained value. The shift in position of triangular equilibrium points as obtained numerically is much more pronounced compared to the analytical predictions. As the value of q_2 is increased, the difference in the analytically and numerically calculated value was found to be larger.

On observing, the Figures 3 and 5, we conclude that the analytical approximation of the triangular equilibrium is more accurate when studied as

Binary Systems	Mass ratio (μ)	q_1	q_2	Collinear points	Triangular points
(η Cas)	0.258126	0.99	1	$L_1(0.183787, 0)$, $L_2(1.239, 0)$, $L_3(-1.14772, 0)$	$(0.127011, \pm 0.864089)$
			0.9	$L_1(0.195437, 0)$, $L_2(1.21647, 0)$, $L_3(-1.14463, 0)$	$(0.160926, \pm 0.843689)$
			0.8	$L_1(0.208286, 0)$, $L_2(1.19229, 0)$, $L_3(-1.14155, 0)$	$(0.196124, \pm 0.820501)$
		1	0.99	$L_1(0.186133, 0)$, $L_2(1.23734, 0)$, $L_3(-1.15016, 0)$	$(0.133689, \pm 0.864089)$
		0.9		$L_1(0.173255, 0)$, $L_2(1.23203, 0)$, $L_3(-1.12185, 0)$	$(0.099774, \pm 0.843689)$
		0.8		$L_1(0.158881, 0)$, $L_2(1.22674, 0)$, $L_3(-1.09143, 0)$	$(0.064576, \pm 0.820501)$
($Gliese$ 65)	0.6185	0.99	1	$L_1(0.00756609, 0)$, $L_2(1.20013, 0)$, $L_3(-1.19375, 0)$	$(0.00285943, \pm 0.864089)$
			0.9	$L_1(0.0198918, 0)$, $L_2(1.17465, 0)$, $L_3(-1.18961, 0)$	$(0.0367746, \pm 0.843689)$
			0.8	$L_1(0.0335572, 0)$, $L_2(1.14728, 0)$, $L_3(-1.18549, 0)$	$(0.0719725, \pm 0.820501)$
		1	0.99	$L_1(0.00993013, 0)$, $L_2(1.19808, 0)$, $L_3(-1.19584, 0)$	$(0.00953726, \pm 0.864089)$
		0.9		$L_1(-0.00245286, 0)$, $L_2(1.19384, 0)$, $L_3(-1.17008, 0)$	$(-0.0243779, \pm 0.843689)$
		0.8		$L_1(-0.0161892, 0)$, $L_2(1.18961, 0)$, $L_3(-1.14242, 0)$	$(-0.0595758, \pm 0.820501)$

Table 2. Equilibrium points for (η Cas) system and $Gliese$ 65 system when the radiation pressure is varied.

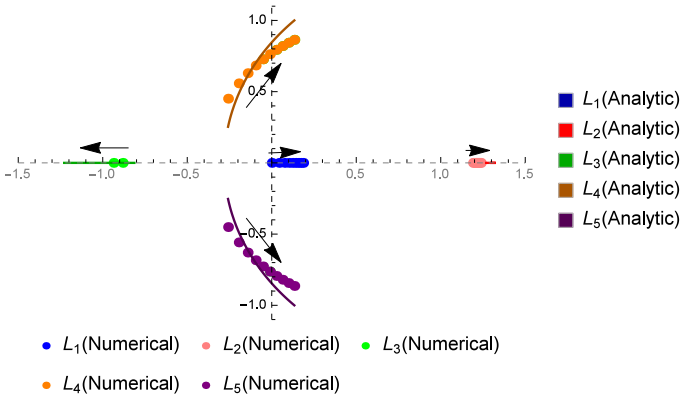

Fig. 3. The shift in the planar equilibrium points for (η *Cas*) system when q_1 is changed from 0.1 to 1 and $q_2 = 0.99$. The dots denote the points corresponding to the numerical calculation whereas the solid line shows the shift in position corresponding to analytically obtained expression.

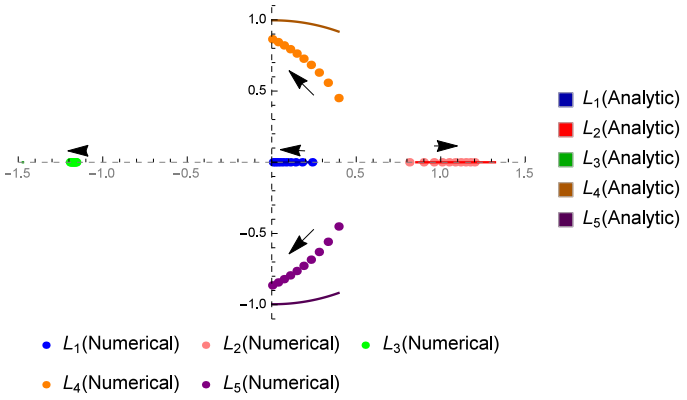

Fig. 4. The shift in the planar equilibrium points for *Gliese* 65 system when q_2 is changed from 0.1 to 1 and $q_1 = 0.99$. The dots denote the points corresponding to the numerical calculation whereas the solid line shows the shift in position corresponding to analytically obtained expression.

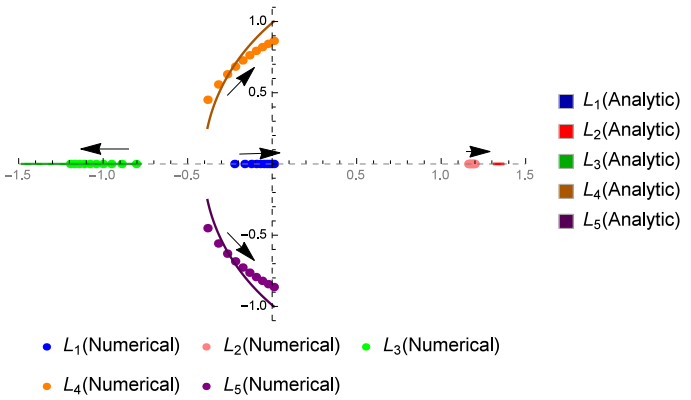

Fig. 5. The shift in the planar equilibrium points for *Gliese* 65 system when q_1 is changed from 0.1 to 1 and $q_2 = 0.99$. The dots denote the points corresponding to the numerical calculation whereas the solid line shows the shift in position corresponding to analytically obtained expression.

function of q_1. Whereas the analytical approximation of L_1 is vaguer in these cases.

3 The Hill's curve on the xy-plane

The boundary curves, delimiting the regions of possible motion and forbidden regions for the movement of the third body in a restricted three-body problem on a plane $O\bar{x}\bar{y}$, or a plane $O\bar{x}\bar{z}$, are known as Zero-velocity curves, or Hill's curves. A Hill's curve is obtained by taking a cross-section of the potential surface at a specific energy level, corresponding to the Jacobian constant of the third body.

The zero-velocity surfaces(ZVS) in ERTBP (Szebehely [1967], Mako and-Szenkovits [2004]) are given by

$$2\omega(\bar{x}, \bar{y}, \bar{z}, f) = C(f), \tag{6}$$

where,

$$C(f) = (1 + e\cos f)\left(C_0 + e\int_{f_0}^{f} \frac{\bar{z}^2 \sin\theta}{1 + e\cos\theta} d\theta + 2e\int_{f_0}^{f} \frac{\omega \sin\theta}{(1 + e\cos\theta)^2} d\theta\right). \tag{7}$$

The ZVS is of type of an ellipsoid, cylinder or hyperboloid, depending on the sign of $\cos f$. Geometrically, it means that at each value of the true anomaly f, a different set of surfaces of zero velocity are to be constructed. The shape and dimension of these zero velocity surfaces vary with true-anomaly, thus for ERTBP they are named as pulsating ZVS.

The necessary conditions for the zero velocity surfaces (ZVS) for ERTBP given by (6) are approximated to

$$2\omega^0(\bar{x},\bar{y},\bar{z},f) = C^*(f), \tag{8}$$

where,

$$\omega^0 = \frac{1}{2}\left(\bar{x}^2+\bar{y}^2\right) + \left\{\frac{(1-\mu)q_1}{\bar{r}_1} + \frac{\mu q_2}{\bar{r}_2}\right\};$$

and

$$C^*(f) = (1+e\cos f)C_0.$$

Therefore, the necessary conditions for the bifurcation, based on Hill's region (Mako and Szenkovits [2004]) are as follows:

1. For the initial condition $(f_0,\ \mathbf{x}_0)$, if the infinitesimal mass is outside the Hill-zone surrounding the second primary and satisfies the condition $C_2 < C_0^* \frac{1-e}{1+e\cos f_0}$, it is never captured by S_2.
2. For the initial condition $(f_0,\ \mathbf{x}_0)$, if the infinitesimal mass is in the exterior of the complete Hill-zone and satisfies the condition $C_1 < C_0^* \frac{1-e}{1+e\cos f_0}$, it never enters the Hill zone surrounding S_2.

Here C_1 and C_2 are constants corresponding to collinear equilibrium points L_1 and L_2, respectively.

For each value of the true anomaly these surfaces admits two planes of symmetry: $\bar{z}=0$ and $\bar{y}=0$. The projection of the pulsating zero-velocity surfaces on the $O\bar{x}\bar{y}-$plane, corresponding to Jacobi constant for the planar equilibrium points, are represented in Figures 6 to 29.

The zero-velocity curves depicted in the Figures 6-9 for the binary system ($\eta\ Cas$) correspond to Jacobi constant, calculated at the three collinear points c_1 to c_3, and the pair triangular points c_4 for the fixed values $q_1 = q_2 = 0.99$. These figures show the pulsation of the ZVC with respect to the true anomaly f. The value of f is taken from 0 to the value for which delimiting curves are observed. It can be seen, that in each case of c_i for $f = 0$, three curves are observed. The large circle encloses both the primaries and the equilibrium points and the smaller circles encloses the primaries. As f increases, the large circle shrinks, where as the internal curve opens up to form a horseshoe then tadpoles, surrounding the triangular equilibrium points. The value of f at which the curves open up is different for varying value of the Jacobi constant.

Similarly, the Figures 10-13 show the pulsating ZVC for the binary system *Gliese* 65. In the case of *Gliese* 65, the large circle encloses both the primaries and the equilibrium points, and two smaller circles of equal radii are surrounding the primaries. As f increases, the large circle shrinks, where as the internal circle slowly expands and opens up to form tadpoles surrounding the triangular equilibrium points corresponding to Jacobi constants C_3 and C_4, respectively. However, for Jacobi constants C_1 and C_2, the circles shrink in size, but do not change shape.

Figures 14 to 17 show the change in the shape of the ZVC when the value of q_1 is decreased from 0.99 to 0.09 for the ($\eta\ Cas$) system, and Figures 22 to

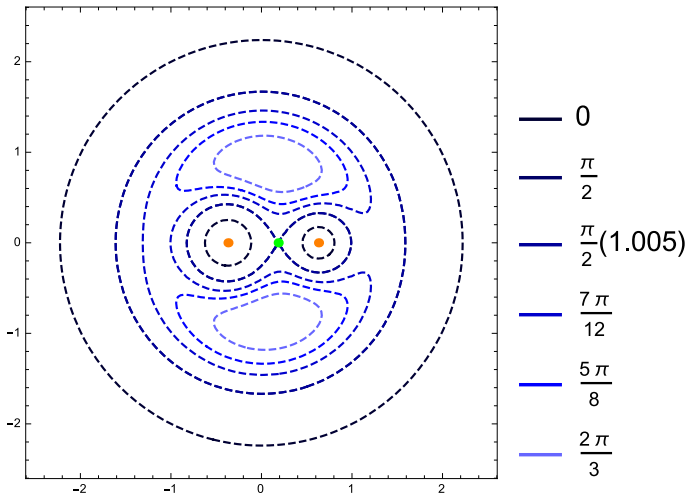

Fig. 6. Variation in Zero velocity curve, corresponding to when the Jacobi constant is taken to be c_1 for varying value of the true anomaly when $q_1 = q_2 = 0.99$ for the (η Cas) system.

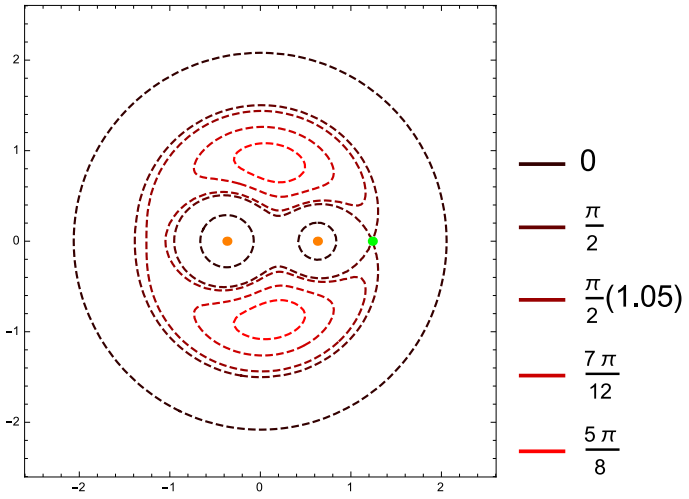

Fig. 7. Variation in Zero velocity curve, corresponding to when the Jacobi constant is taken to be c_2 for varying value of the true anomaly when $q_1 = q_2 = 0.99$ for the (η Cas) system.

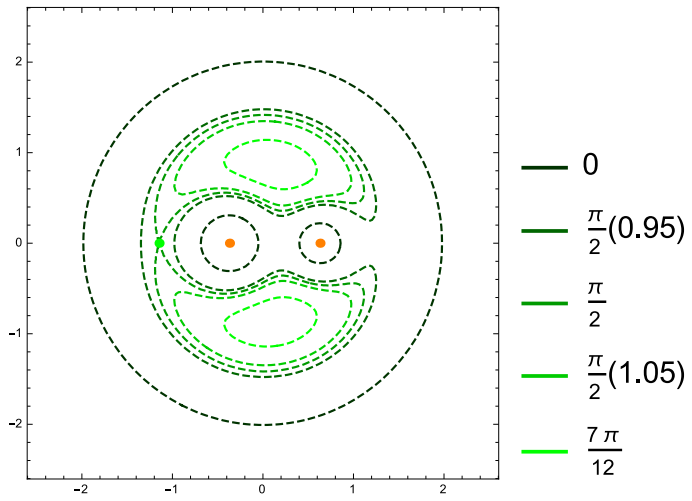

Fig. 8. Variation in Zero velocity curve, corresponding to when the Jacobi constant is taken to be c_3 for varying value of the true anomaly when $q_1 = q_2 = 0.99$ for the (η Cas) system.

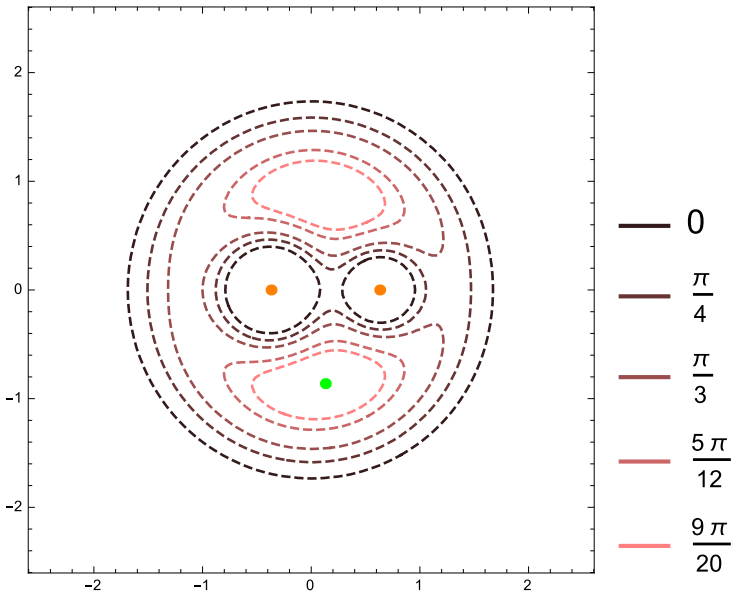

Fig. 9. Variation in Zero velocity curve, corresponding to when the Jacobi constant is taken to be c_4 for varying value of the true anomaly when $q_1 = q_2 = 0.99$ for the (η Cas) system.

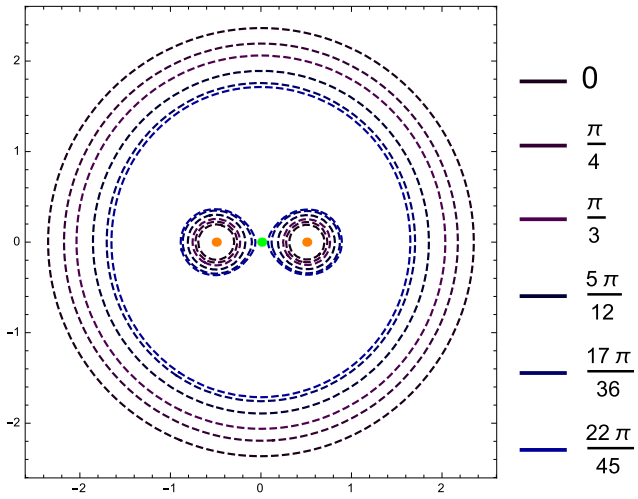

Fig. 10. Variation in Zero velocity curve, corresponding to when the Jacobi constant is taken to be c_1 for varying value of the true anomaly when $q_1 = q_2 = 0.99$ for the *Gliese*65 system.

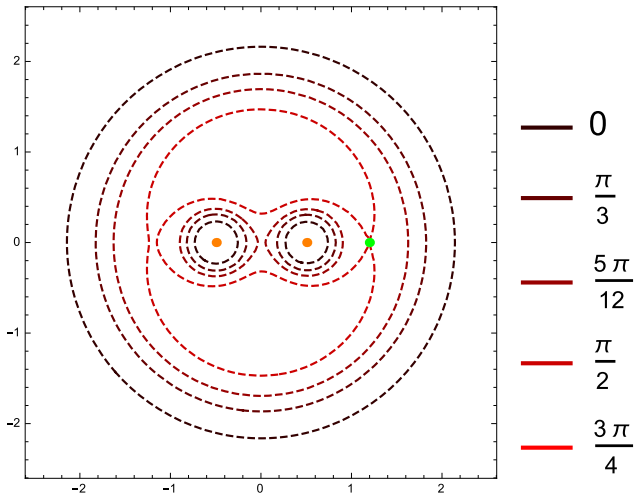

Fig. 11. Variation in Zero velocity curve, corresponding to when the Jacobi constant is taken to be c_2 for varying value of the true anomaly when $q_1 = q_2 = 0.99$ for the *Gliese*65 system.

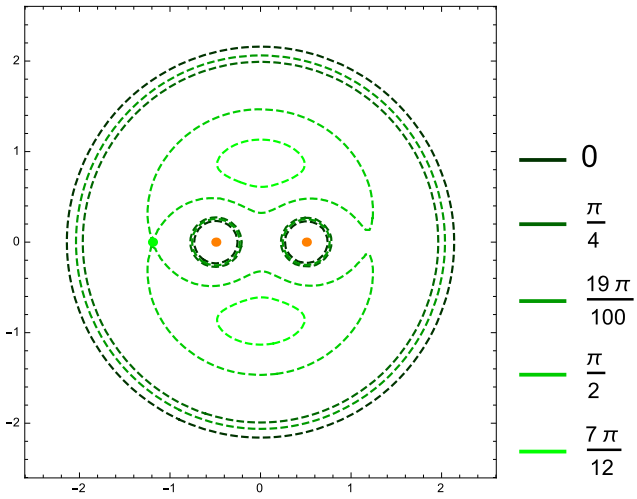

Fig. 12. Variation in Zero velocity curve, corresponding to when the Jacobi constant is taken to be c_3 for varying value of the true anomaly when $q_1 = q_2 = 0.99$ for the *Gliese*65 system.

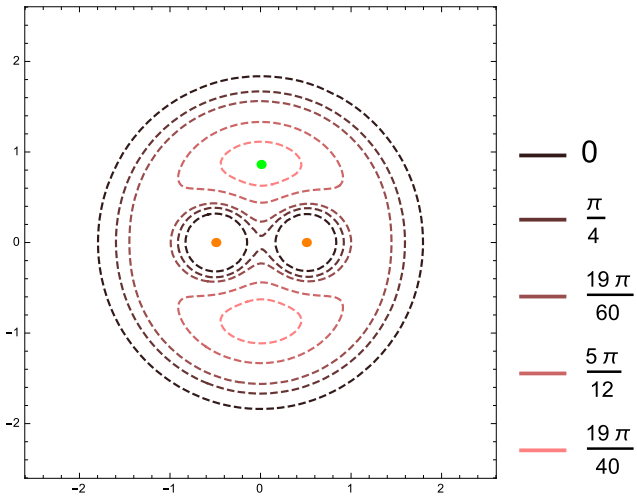

Fig. 13. Variation in Zero velocity curve, corresponding to when the Jacobi constant is taken to be c_4 for varying value of the true anomaly when $q_1 = q_2 = 0.99$ for the *Gliese*65 system.

25 show the change in the shape of the ZVC for *Gliese* 65 system, respectively. The horseshoe-shaped curve shrinks in size with the decrease in value of q_1 corresponding to c_1 and c_4. In case of the Jacobi constants c_2 and c_3, the change in the size of the curve is accompanied by a change in shape. Similar changes are observed for both the systems. Figures 18 - 21 and 26 -29 show the change in the shape of the ZVC when the value of q_2 is decreased from 0.99 to 0.09 for (η Cas) and *Gliese* 65, respectively. For all four Jacobi constants, the decrease in size of the curve is accompanied by a change in shape.

Thus, we observe the phenomenon of pulsating ZVC for the binary systems, and both the shape and size of the forbidden regions are affected by the radiation pressure of the binaries.

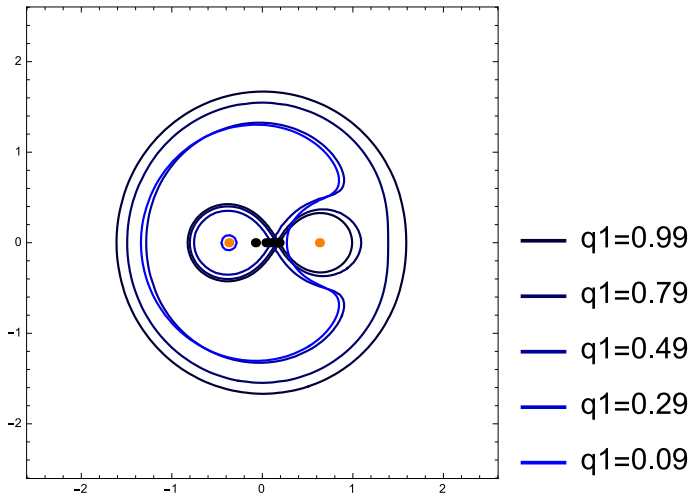

Fig. 14. Variation in Zero velocity curve, corresponding to c_1 for varying value of q_1, when $q_2 = 0.99$ for (η Cas) system.

4 Fractal Basin

The fractal basin of attraction of a point (attractor) refers to the region from which each point tends towards the point after several iterations. This basin of attraction of equilibrium point is used to choose an initial point for periodic orbits around the equilibrium point. An initial point, chosen from inside the region of attraction, increases the possibility of getting a stable orbit. However, the initial point, chosen among the boundary values, shows chaotic behavior.

The multi-variate version of Newton-Raphson's method is employed to get the basin of attraction of the planar equilibrium points because of its high rate of convergence.

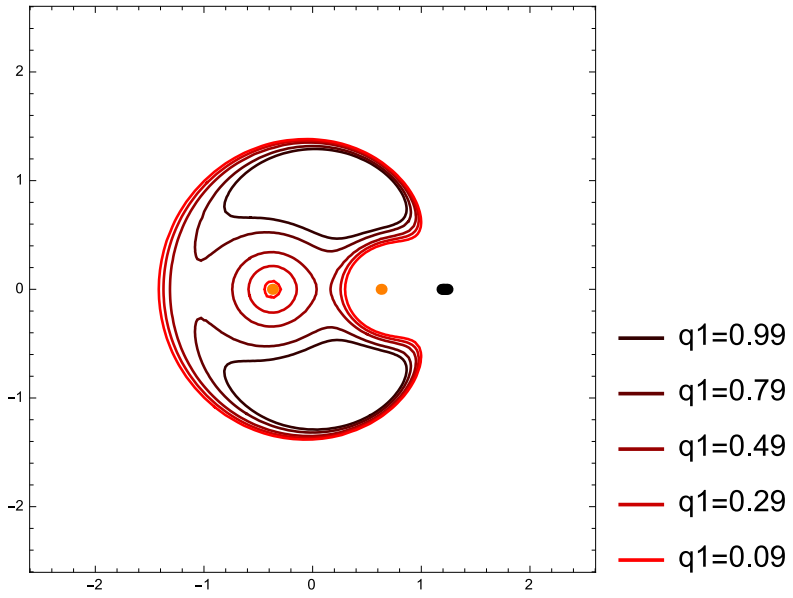

Fig. 15. Variation in Zero velocity curve, corresponding to c_2 for varying value of q_1, when $q_2 = 0.99$ for (η Cas) system.

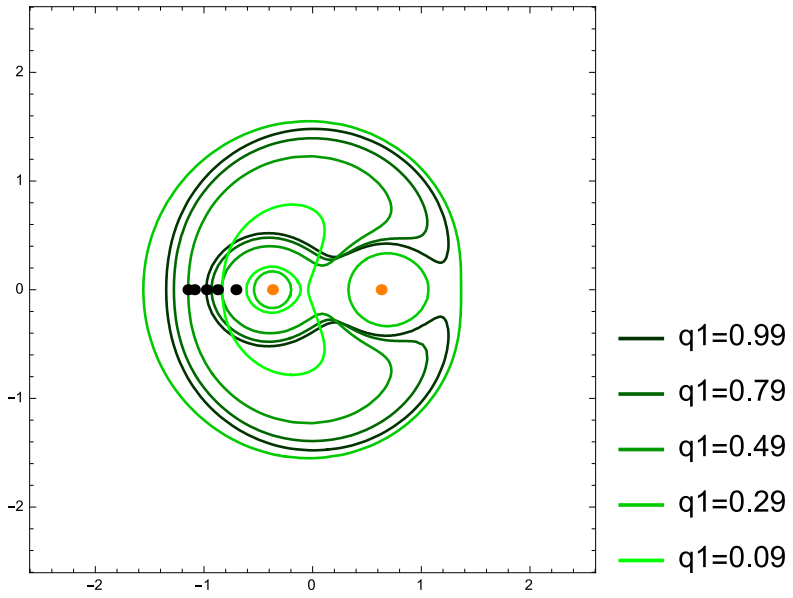

Fig. 16. Variation in Zero velocity curve, corresponding to c_3 for varying value of q_1, when $q_2 = 0.99$ for (η Cas) system.

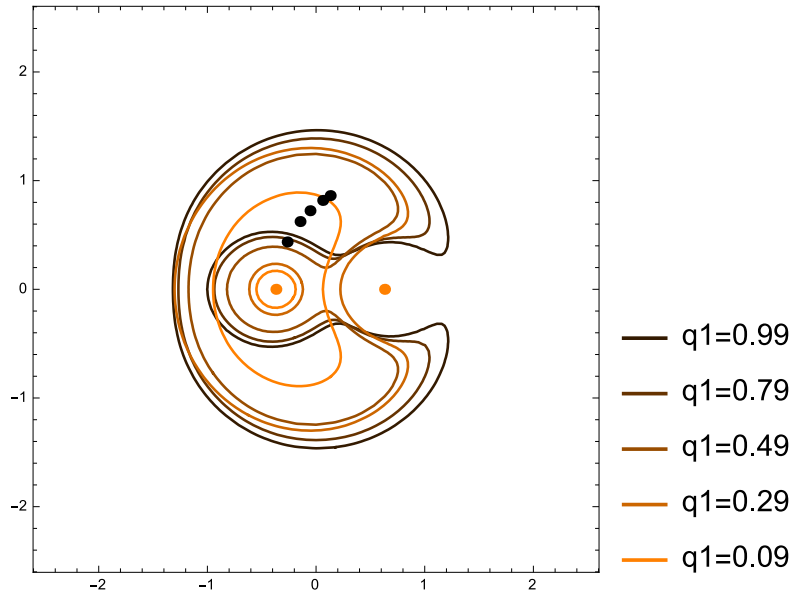

Fig. 17. Variation in Zero velocity curve, corresponding to c_4 for varying value of q_1, when $q_2 = 0.99$ for $(\eta\ Cas)$ system.

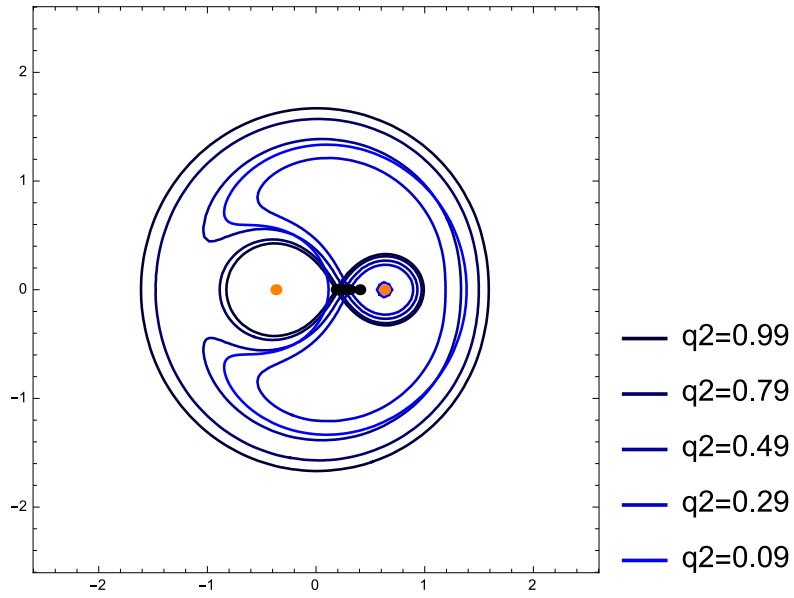

Fig. 18. Variation in Zero velocity curve, corresponding to c_1 for varying value of q_2, when $q_1 = 0.99$ for $(\eta\ Cas)$ system.

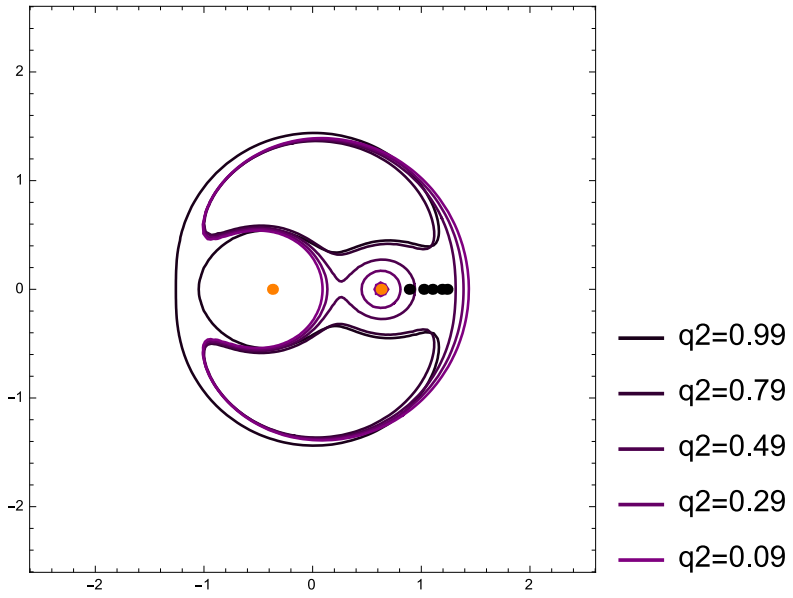

Fig. 19. Variation in Zero velocity curve, corresponding to c_2 for varying value of q_2, when $q_1 = 0.99$ for (η Cas) system.

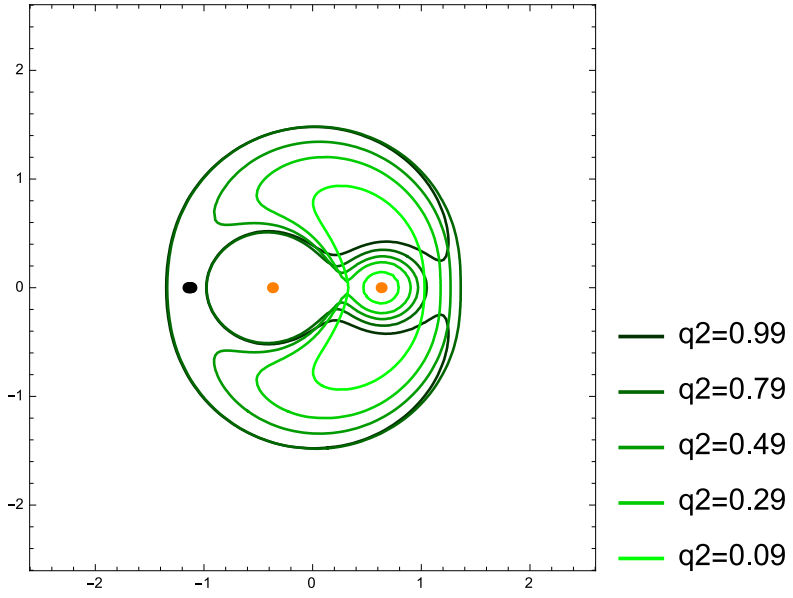

Fig. 20. Variation in Zero velocity curve, corresponding to c_3 for varying value of q_2, when $q_1 = 0.99$ for (η Cas) system.

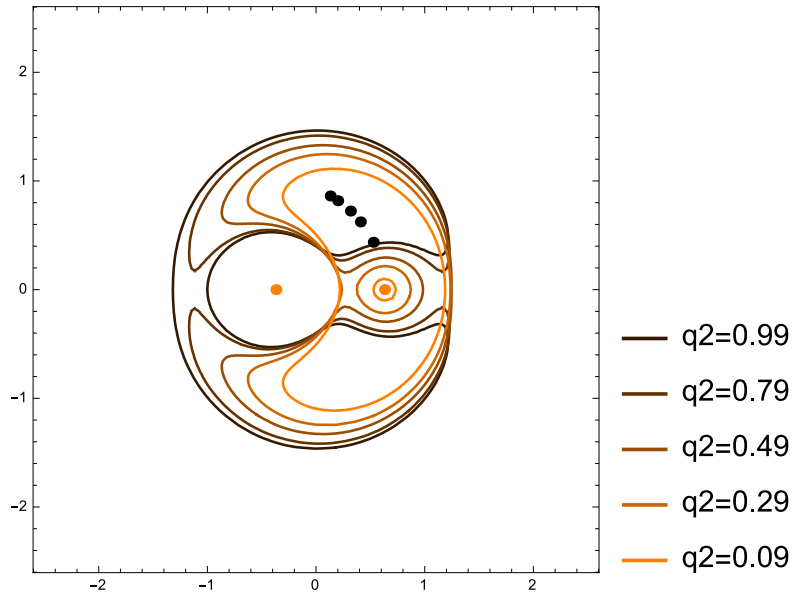

Fig. 21. Variation in Zero velocity curve, corresponding to c_4 for varying value of q_2, when $q_1 = 0.99$ for $(\eta\ Cas)$ system.

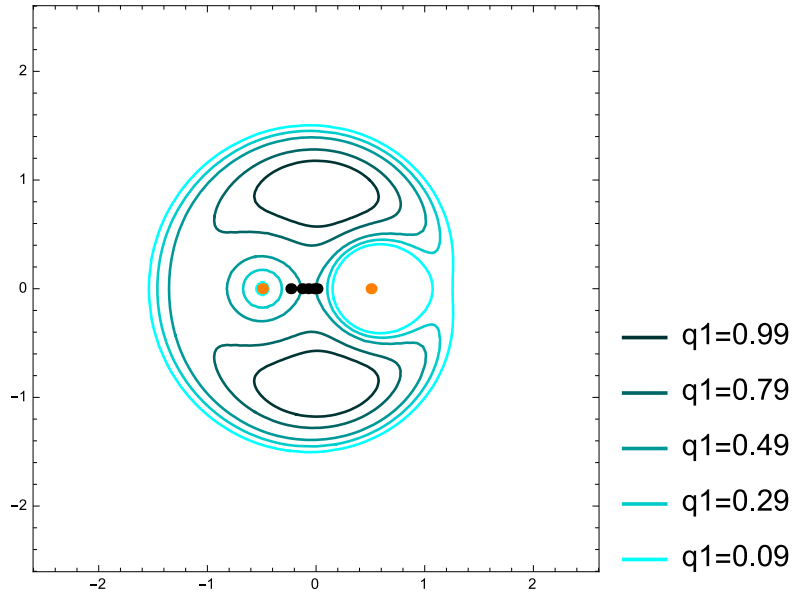

Fig. 22. Variation in Zero velocity curve, corresponding to c_1 for varying value of q_1, when $q_2 = 0.99$ for $Gliese65$ system.

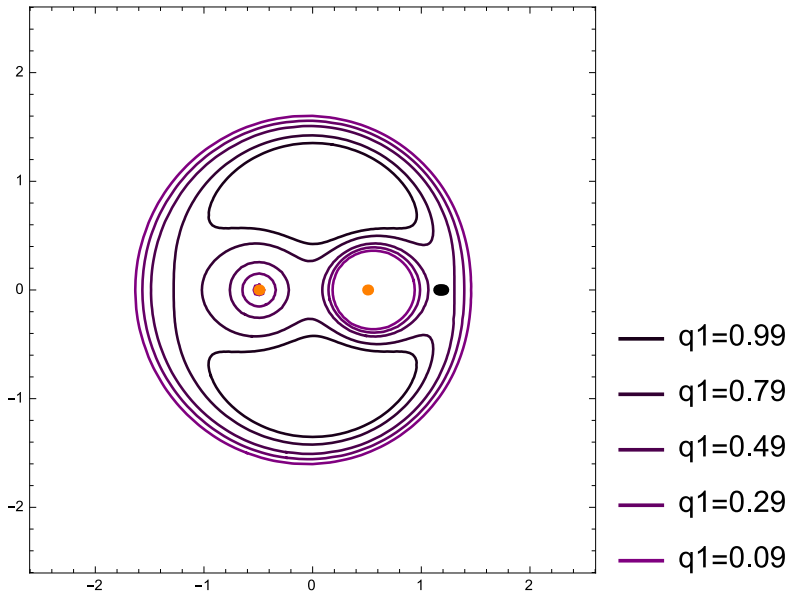

Fig. 23. Variation in Zero velocity curve, corresponding to c_2 for varying value of q_1, when $q_2 = 0.99$ for *Gliese*65 system.

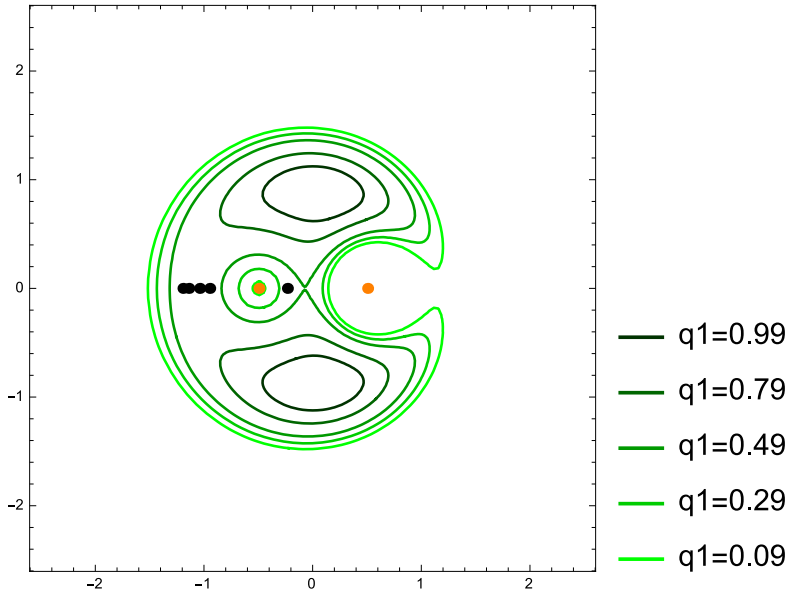

Fig. 24. Variation in Zero velocity curve, corresponding to c_3 for varying value of q_1, when $q_2 = 0.99$ for *Gliese*65 system.

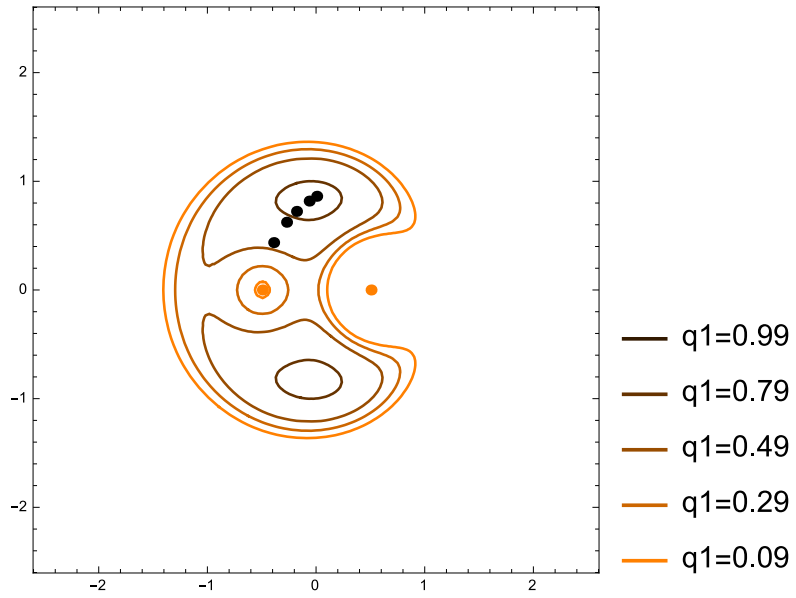

Fig. 25. Variation in Zero velocity curve, corresponding to c_4 for varying value of q_1, when $q_2 = 0.99$ for *Gliese*65 system.

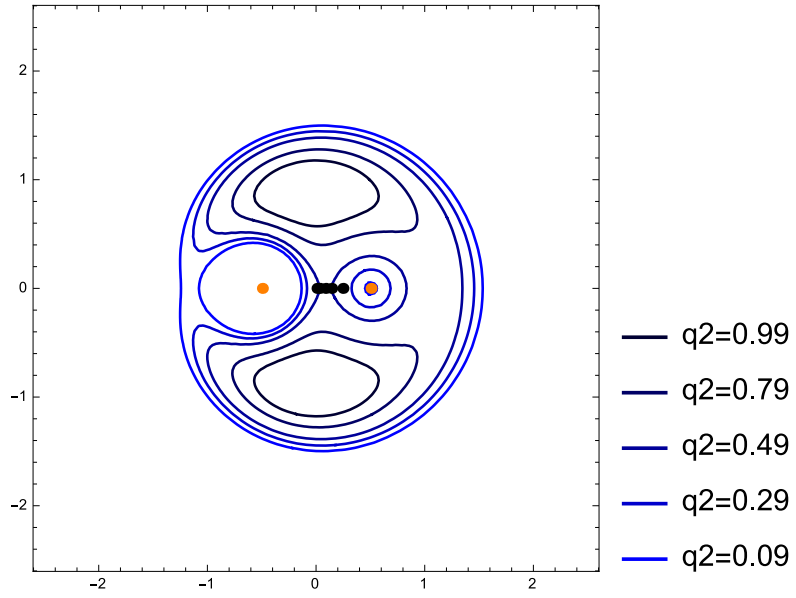

Fig. 26. Variation in Zero velocity curve, corresponding to c_1 for varying value of q_2, when $q_1 = 0.99$ for *Gliese*65 system.

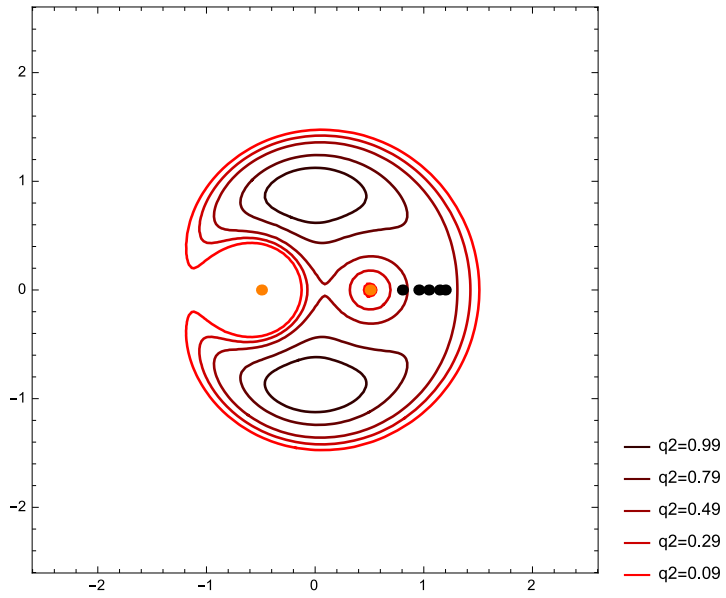

Fig. 27. Variation in Zero velocity curve, corresponding to c_2 for varying value of q_2, when $q_1 = 0.99$ for *Gliese*65 system.

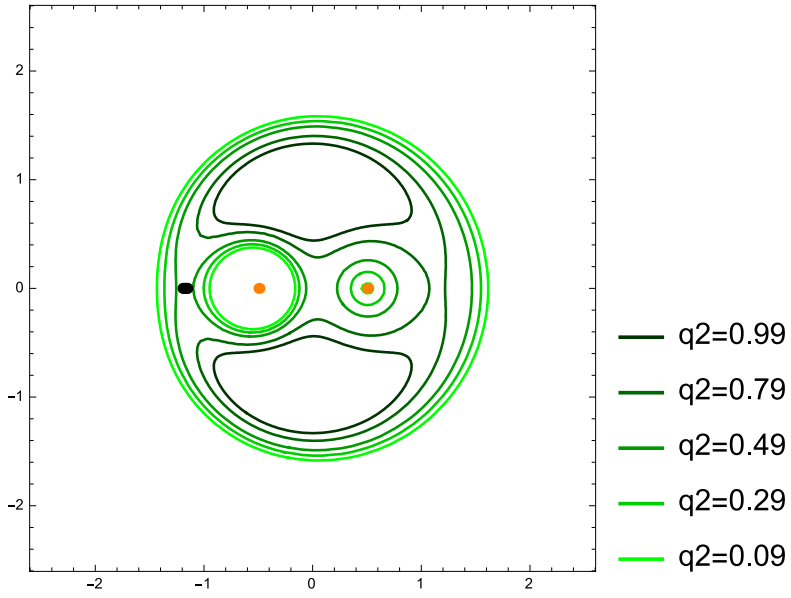

Fig. 28. Variation in Zero velocity curve, corresponding to c_3 for varying value of q_2, when $q_1 = 0.99$ for *Gliese*65 system.

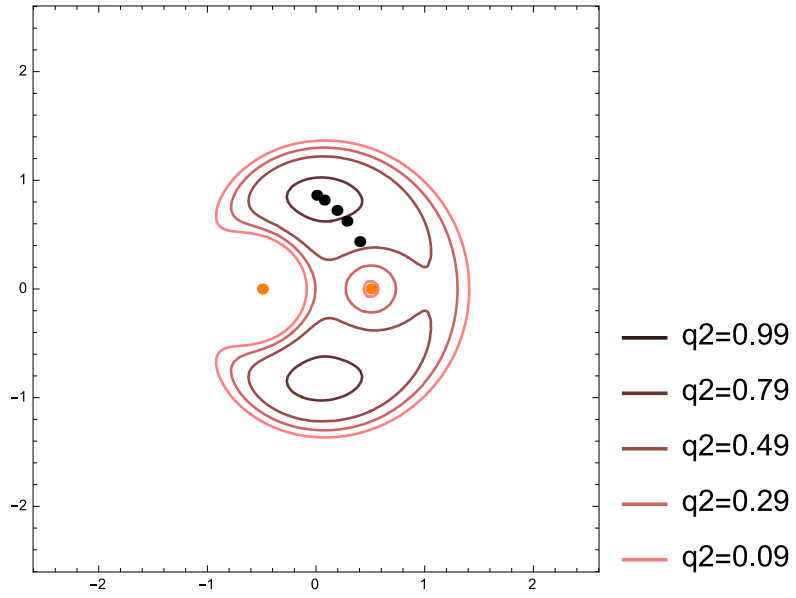

Fig. 29. Variation in Zero velocity curve, corresponding to c_4 for varying value of q_2, when $q_1 = 0.99$ for $Gliese65$ system.

The iterative scheme, used to get the basin of attraction for each planar equilibrium point in the $\bar{x}\bar{y}$ plane, is as follows:

$$\bar{x}_{n+1} = \bar{x}_n - \left(\frac{\Omega_{\bar{x}}\Omega_{\bar{y}\bar{y}} - \Omega_y \Omega_{\bar{x}\bar{y}}}{\Omega_{\bar{x}\bar{x}}\Omega_{\bar{y}\bar{y}} - \Omega^2_{\bar{x}\bar{y}}} \right)_{(\bar{x}_n, \bar{y}_n)} ;$$

$$\bar{y}_{n+1} = \bar{y}_n + \left(\frac{\Omega_{\bar{x}}\Omega_{\bar{y}\bar{x}} - \Omega_{\bar{y}}\Omega_{\bar{y}\bar{y}}}{\Omega_{\bar{x}\bar{x}}\Omega_{\bar{y}\bar{y}} - \Omega^2_{\bar{x}\bar{y}}} \right)_{(\bar{x}_n, \bar{y}_n)} ;$$

where,

$$\Omega_{\bar{x}} = \frac{1}{1 + e\cos f} \left(\bar{x} - \frac{q_1(1-\mu)(\bar{x}+\mu)}{\bar{r}_1^3} - \frac{q_2\mu(\bar{x}+\mu-1)}{\bar{r}_2^3} \right),$$

$$\Omega_{\bar{y}} = \frac{1}{1 + e\cos f} \left(\bar{y} - \frac{q_1(1-\mu)\bar{y}}{\bar{r}_1^3} - \frac{q_2\mu\bar{y}}{\bar{r}_2^3} \right),$$

$$\Omega_{\bar{x}\bar{x}} = \frac{1}{1+e\cos f}\left(1 - \frac{q_1(1-\mu)}{\bar{r}_1^3} - \frac{q_2\mu}{\bar{r}_2^3} + \frac{3q_1(1-\mu)(\bar{x}+\mu)^2}{\bar{r}_1^5} + \frac{3q_2\mu(\bar{x}+\mu-1)^2}{\bar{r}_2^5}\right),$$

$$\Omega_{\bar{x}\bar{y}} = \frac{1}{1+e\cos f}\left(\frac{3q_1(1-\mu)(\bar{x}+\mu)\bar{y}}{\bar{r}_1^5} + \frac{q_2\mu(\bar{x}+\mu-1)\bar{y}}{\bar{r}_2^5}\right),$$

$$\Omega_{\bar{y}\bar{y}} = \frac{1}{1+e\cos f}\left(1 - \frac{q_1(1-\mu)}{\bar{r}_1^3} - \frac{q_2\mu}{\bar{r}_2^3} + \frac{3q_1(1-\mu)\bar{y}^2}{\bar{r}_1^5} + \frac{3q_2\mu\bar{y}^2}{\bar{r}_2^5}\right).$$

The initial conditions for the position that iterates to the particular planar equilibrium position is depicted as the Newton–Raphson basins of attraction (BoA). The double scanning technique is used to find these regions on $O\bar{x}\bar{y}$ plane. Here, we have considered the intervals $-3.0 \leq \bar{x} \leq 3.0$ and $-3.0 \leq \bar{y} \leq 3.0$ for the vertical and the horizontal scanning, respectively, and 10 iterations were applied with step size of 0.005. In the Figures 30 - 33 the color coded diagrams in the $O\bar{x}\bar{y}$- plane are shown. Figures 31 and 33 have four sub-figures, the basins of attraction for (η Cas) and $Gliese$ 65 system for varying values of radiation pressure of the primaries.

The BoAs for the equilibrium points L_2 and L_3 are bug like structures flaring out as two sub-parts densely formed about the equilibrium point, whereas the BoAs for the equilibrium points L_4 and L_5 are wing like structures and also it forms an extension of the legs of the bug-like structures of L_2 and L_3. The points of the rest of the sub-plane $-3.0 \leq \bar{x} \leq 3.0,\ -3.0 \leq \bar{y} \leq 3.0$ converges to L_1. The boundary of the BoA for all the equilibrium points is very fractus and shows very small regions converging to other equilibrium point.

Figures 30 and 32 shows the Newton–Raphson basins of attraction for (η Cas) and $Gliese$ 65 when radiation pressure of both the primaries is assumed to be 0.99. On inspecting the Figures 30, 31(a) and 31(c), for the (η Cas), we found that the BoA, corresponding to all the equilibrium points except L_1, decrease in size. However, the shape of none of the basins change with decrease in the value of q_1. When the value of q_2 is decreased, the symmetry of BoA of L_1 near this point looses its symmetry as observed from Figures 30, 31(b) and 31(d).

Inspecting Figure 32 we note that the BoA of the equilibrium points L_2 and L_3 for the $Gliese$ 65 system are symmetrical about the $x-$ axis and the equilibrium points L_1, L_4 and L_5 are symmetrical about the $y-$ axis. From Figures 32, 33(a) and 33(c), we note that when q_1 is decreased, the BoA of L_3 contracts. Also, the BoA for L_1, L_4 and L_5 to the left of the $y-$ axis is squeezed and looses its symmetry. Similar phenomenon is observed for the case when q_2 is decreased for the equilibrium points L_2 and L_1, L_4 & L_5, respectively.

5 Discussion and Conclusion

A system of two massive objects orbiting in elliptical orbits is used as a model for studying the dynamics of an infinitesimal mass in the vicinity of two binary systems, η Cas and $Gliese$ 65. In this paper we have employed the model of the elliptic restricted three-body problems, replacing the well studied circular restricted model, since most of the celestial bodies are known to be orbiting in elliptic orbits and not circular orbits. Therefore, the perturbation caused by

Fig. 30. Fractal basin for (η *Cas*) system when $q_1 = q_2 = 0.99$. Here, the BoA for each equilibrium point is coded in different colors as follows: L_1-Prurple, L_2-Blue, L_3-Green, L_4-Red and L_5-Yellow. The black dots are depicting the equilibrium points.

the non-zero eccentricity of the orbits of massive bodies makes the long-term dynamical studies more precise.

The motivations behind this study are as follows:

1. Binary star systems are common in the universe, and their dynamics can provide insights into the formation and evolution of stars.

2. The study of equilibrium points helps in predicting the characteristics of the gravitational waves emitted by these systems, aiding in their detection and analysis by gravitational wave observatories like LIGO and VIRGO.

3. The study of equilibrium points in binary star systems contributes to our understanding of how stars form within stellar nurseries.

We have compared analytical and numerical results for the position of equilibrium points and depicted them in graphs. It was observed that in congruence to the analytically obtained expressions for the position of equilibrium points, the numerical study also showed that the equilibrium points are dependent on the radiation pressure of radiating primaries, which acts as the mass reduction factor for that primary. All the equilibrium points are affected by the radiation pressure of primaries, namely q_1 and q_2. The most shifted equilibrium point for decrease in q_1 is L_4, L_5 and L_3. Similarly, the decrease in q_2 has an impressive effect on the shift in position of L_4, L_5 and L_2.

We note that the shift in position of the collinear point L_1, as obtained as a function of q_2, is almost coincidental with numerical results for both systems. But the analytic value of the collinear points L_2 and L_3 is an overestimation of the numerically obtained value. The shift in position of triangular equilibrium points, as obtained numerically, is much more pronounced as compared

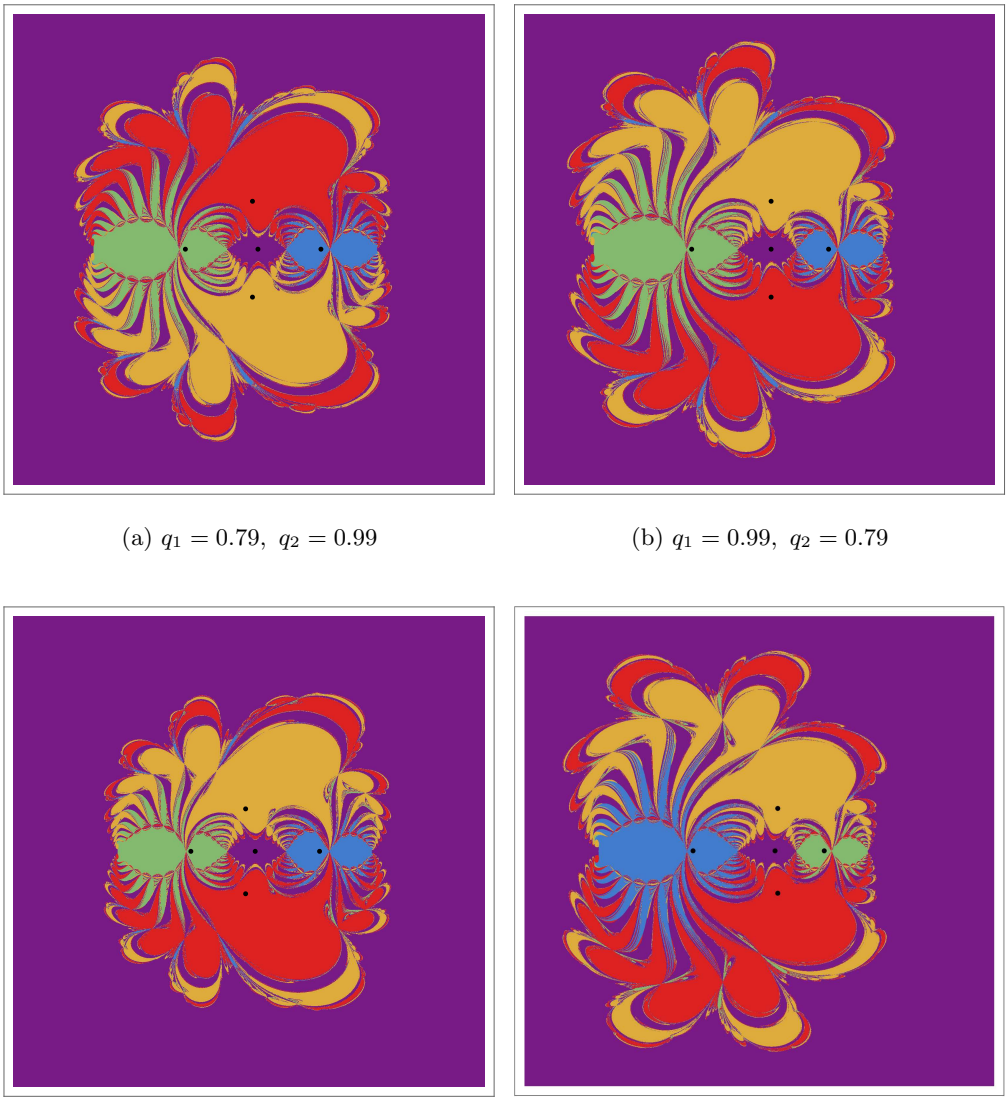

(a) $q_1 = 0.79,\ q_2 = 0.99$

(b) $q_1 = 0.99,\ q_2 = 0.79$

(c) $q_1 = 0.49,\ q_2 = 0.99$

(d) $q_1 = 0.99,\ q_2 = 0.49$

Fig. 31. Fractal basin for $(\eta\ Cas)$ system varying the values of q_1 and q_2.

Fig. 32. Fractal basin for *Gliese* 65 system when $q_1 = q_2 = 0.99$. Here, the BoA for each equilibrium point is coded in different colors as follows: L_1-Red, L_2-Yellow, L_3-Green, L_4-Blue and L_5-Purple. The black dots are depicting the equilibrium points.

to the analytical predictions. When the value of q_2 is increased, the approximation error was found to increase too. Also, we conclude that the analytical approximation of the triangular equilibrium is more accurate when studied as a function of q_1, whereas the analytical approximation of L_1 is vaguer in these cases.

Further, we used numerically obtained positions of the equilibrium points. On studying the ZVC for the two binary systems, it was seen that curves pulsate with the change in true anomaly, and both radiation pressure of the first and second primary causes the change in shape and size of the forbidden regions. We observe that in each case of c_i for $f = 0$, two curves are observed. For the (η *Cas*) system, a large circle encloses both the primaries and the equilibrium points. As f increases, the large circle shrinks, whereas the internal curve opens up to form a horseshoe, then tadpoles surrounding the triangular equilibrium points. The value of f at which the curves open up is different because of the varying value of the Jacobi constant.

In the case of the *Gliese* 65 system, a large circle encloses both the primaries and the equilibrium points, and two smaller circles surround the primaries. As f increases, the large circle shrinks, whereas the internal circle slowly enlarges and opens up to form tadpoles surrounding the triangular equilibrium points.

Studying the effect of radiation pressure on ZVC, we observed when q_1 is decreased from 0.99 to 0.09 for both systems, the horseshoe-shaped curve shrinks in size corresponding to c_1 and c_4, in case of the Jacobi constants c_2 and c_3 change in the size of curve is accompanied by a change in shape. When the value of q_2 is decreased from 0.99 to 0.09 for (η *Cas*) and *Gliese* 65

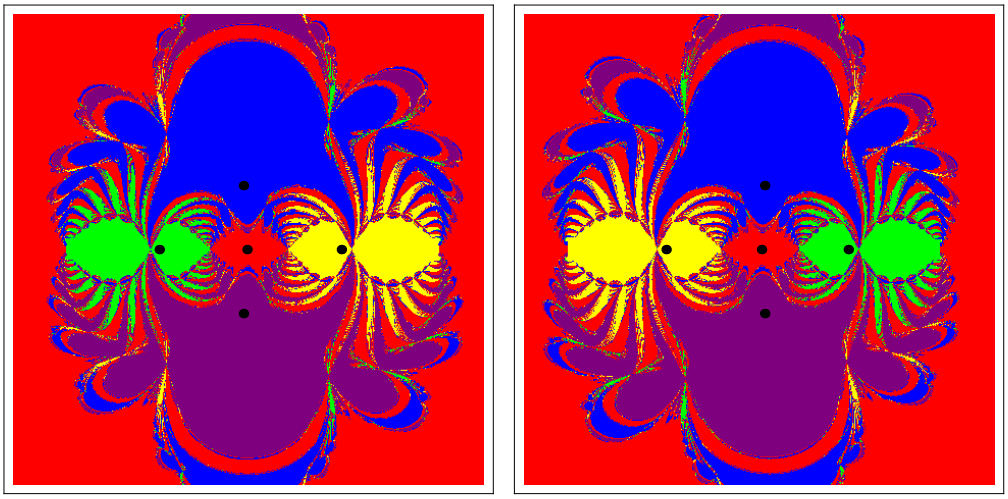

(a) $q_1 = 0.79,\ q_2 = 0.99$ (b) $q_1 = 0.99,\ q_2 = 0.79$

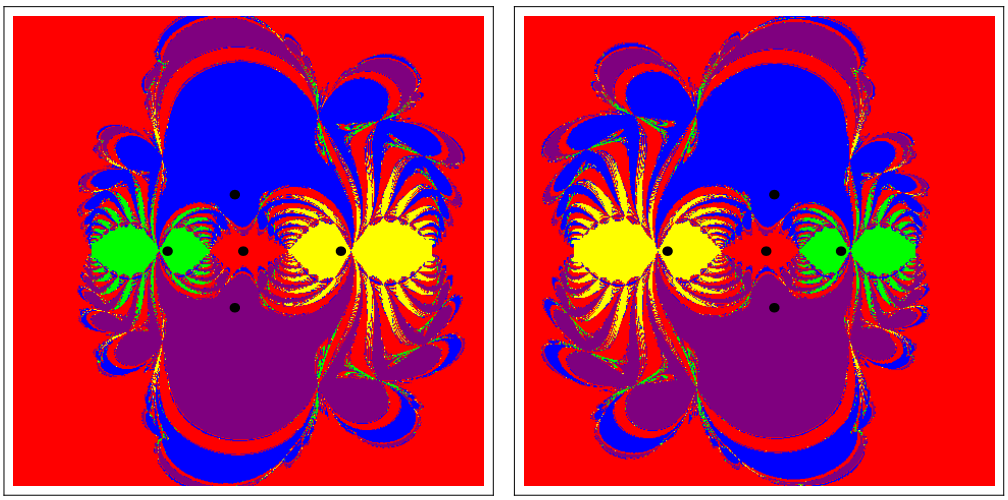

(c) $q_1 = 0.49,\ q_2 = 0.99$ (d) $q_1 = 0.99,\ q_2 = 0.49$

Fig. 33. Fractal basin for *Gliese* 65 system varying the values of q_1 and q_2.

systems, respectively, for all four Jacobi constants, the decrease in size of the forbidden region is accompanied by a change in shape.

The color-coded plots of the basin of attraction of the five equilibrium points for the systems $\eta\ Cas$ and *Gliese* 65 are presented in the previous section. They show small change in the size of the BoA and its symmetry (in the case of L_1), with a decrease in the value of radiation pressure for the $\eta\ Cas$ system. For *Gliese* 65 system, the decrease in the value of both q_1 and q_2 shows a prominent effect on the size and symmetry of the BoA for L_2 to L_5. Thus, we conclude that when the radiation pressure decreases, the region from which initial points for stable orbits can be started decreases except for the collinear point L_1.

References

Alrebdi, H.I., Smii, B., Zotos, E. E., 2022, *Results Phys.*, 34, 105240. https://doi.org/10.1016/j.rinp.2022.105240

Aliroma, W. , Maboud, A., Abdel-Salam, F.A., Khatab, H.E., 2019, *Open Astron.*, 28(1), 145

Alzahrani, F., Abouelmagd, E. I., Guirara, J. I. G., Hobiny, A., 2017, *Open Phys.*, 15(1), 58

Ammar, M. K., 2008, *Astrophys. Space Sci.*, 313, 393.

Bhatnagar, K.B., Chawla, J.M., 1979, *Indian J. Pure Appl. Math.*, 10, 1443

Danby, J.M.A., 1964, *Astron. J.*, 69, 165

Kalantonis, V.S., Perdios, E.A., Ragos, O., 2006, *Astrophys. Space Sci.*, 301, 157

Kalantonis, V.S., Perdios, E.A., Perdiou, A.E., 2008, *Astrophys. Space Sci.*, 315, 323

Kumar S. and Ishwar B., 2011, *Int. J. of Eng. Sci. & Tech.*, 3(2), 157

Kumar, C.R., Narayan, A., 2012, *Int. J. Pure Appl. Math.*, 80(4), 477

Kunitsyn, A.L., Perezhogin, A. A., 1978, *Celest. Mech. Dyn. Astron.* 18, 395

Kunitsyn, A.L., Tureshbaev, A.T., 1985, *Celest. Mech. Dyn. Astron.*, 35, 105

Luyten, W. J., 1949, *The Astronomical Journal*, 55, 15. Bibcode:1949AJ.....55...15L. doi:10.1086/106322.

Mako, Z., Szenkovits, F., 2004, *Celest. Mech. Dyn. Astron.*, 90, 51

Narayan, A., Singh, N., 2014, *Astrophys Space Sci.*, 352, 57

Narayan, A., Singh, N., 2014, *Astrophys Space Sci.* 354, 355

Narayan, A., Singh. N., 2014, *Astrophys Space Sci.*, 353(2), 441

Radzievskii V. V., 1950, *Astron. Zh.*, 27, 250

Radzievskii V. V., 1953, *Astron. Zh.*, 30, 265

Selaru, D., Cucu-Dumitrescu, C., 1995, *Celest. Mech. Dyn. Astron.*, 61(4), 333

Schuerman D. W., 1980, *Astrophs. J.*, 238, 337

Singh, J., Haruna, S., 2020, *Sci Rep*, 10, article id. 18861. https://doi.org/10.1038/s41598-020-75174-7

Singh, J., Isah, N., 2021, *Heliyon*, 7(3), article id. e06575, https://doi.org/10.1016/j.heliyon.2021.e06575

Strand, K. A., 1969, *Astronomical Journal*, 74, 760, https://doi:10.1086/110853

Szebehely, V. *Theory of Orbits, The Restricted problem of three bodies. Academic Press, 1967*